Available online at www.sciencedirect.com
SCIENCE DIRECT®
Thermochimica Acta 410 (2004) 149–159
thermochimica acta
www.elsevier.com/locate/tca

A ternary phase diagram of the Mn–Te–O system at 950 K

T.S. Lakshmi Narasimhan, M. Sai Baba, S. Nalini, R. Viswanathan*

Fuel Chemistry Division, Chemical Group, Indira Gandhi Centre for Atomic Research, Kalpakkam, 603 102 Tamil Nadu, India

Received 22 May 2003; received in revised form 29 July 2003; accepted 30 July 2003

Abstract

A ternary phase diagram of the Mn–Te–O system at 950 K has been established in the composition range in and around the MnO–TeO_2 pseudo binary line. Various preparation methods were employed to confirm the co-existence of different ternary phases. The results of these phase equilibration studies were revalidated by the invariancy of partial pressures at constant temperature during high temperature mass spectrometric vaporization experiments. The following three-phase regions have been identified: MnO + Mn_3O_4 + $Mn_6Te_5O_{16}$ (phase region 1; PH1), Mn_3O_4 + $Mn_6Te_5O_{16}$ + $MnTeO_3$ (phase region 2; PH2), Mn_3O_4 + $MnTeO_3$ + Mn_3TeO_6 (phase region 3; PH3), and $MnTeO_3$ + $Mn_2Te_3O_8$ + Mn_3TeO_6 (phase region 4; PH4). The complex nature of the Mn–Te–O ternary system was revealed by the interesting results obtained by us with regard to preparation of samples and mass spectrometric vaporization experiments.

Keywords: Mn–Te–O; Phase diagram; Phase equilibration; Vaporization; Knudsen effusion mass spectrometry

1. Introduction

Recently we have initiated a systematic study of (stainless steel clad component + fission product tellurium + oxygen) ternary systems [1]. This is in continuation of our efforts to generate phase diagram information and thermodynamic data that are relevant to understand the role played by fission product tellurium in the fuel–clad interaction in uranium–plutonium mixed oxide fuelled fast breeder reactors. Earlier, thermodynamic and phase diagram information on the binary systems Fe–Te [2,3], Ni–Te [4], Cr–Te [5,6], Mo–Te [7,8], and Mn–Te [9–11] were generated. Thermodynamic modeling of the available data led to the conclusion [12,13] that fission product tellurium-induced attack becomes important in hyper-stoichiometric uranium–plutonium mixed oxide fuels. Besides the formation of binary tellurides, that of ternary oxide phases involving clad component–tellurium–oxygen, also needs to be considered. Accordingly, we conducted first the studies on the Mn–Te–O system during which we observed the existence of an interesting and not-so-common univariant vaporization equilibrium involving two condensed phases, both ternary [14], but not lying on a single pseudo binary line. In the present paper, we report the studies which led to determination of the Mn–Te–O phase diagram at 950 K in and around the MnO–TeO_2 binary line. A preliminary account of this information has been presented elsewhere [15].

The information available in the literature on the Mn–Te–O system is very limited. Only X-ray, DTA, and calorimetric data exist for some of the tellurite phases around the MnO–TeO_2 pseudo binary line.

Trömel et al. [16] reported preparation of the phases $Mn_6Te_6O_{13}$, $MnTe_2O_5$, $Mn_2Te_3O_8$, $MnTeO_3$, and $Mn_4Te_3O_{10}$ by solid state reactions of MnO and TeO_2. They characterized these compounds by X-ray diffraction (XRD) patterns and indexed the patterns. They also reported the physical properties like appearance, melting, and decomposition temperatures for these compounds. The authors made a special mention of the stability of the phase $Mn_4Te_3O_{10}$ (subsequently re-designated [17] as $Mn_6Te_5O_{16}$). The phase $Mn_6Te_5O_{16}$, on being heated at the same temperature of its preparation (923 K) for longer duration (>10 h), gave rise to generation of $MnTeO_3$ and Mn_3TeO_6 phases, and deposition of elemental tellurium at the colder end of their apparatus, presumably due to the following reaction:

$$3Mn_6Te_5O_{16}(s) \rightarrow 12MnTeO_3(s) + 2Mn_3TeO_6(s) + Te\ (\text{possibly as}\ 0.5Te_2(g)) \quad (1)$$

* Corresponding author. Tel.: +91-4114-280098; fax: +91-4114-280065.
E-mail address: rvis@igcar.ernet.in (R. Viswanathan).

0040-6031/$ – see front matter © 2003 Elsevier B.V. All rights reserved.
doi:10.1016/S0040-6031(03)00399-X

Bayer [18] prepared the phase Mn_3TeO_6(s) by heating MnO(s) and TeO_2(s) in the ratio 3:1 in air for 20 h each at 873 and 973 K, and characterized it by XRD.

Ivanova [19] investigated the MnO–TeO_2 system in the range of 0–50 mol% MnO through DTA, X-ray, and infrared characterization of the samples, which they prepared by melting (MnO + TeO_2) mixtures in an electrical furnace in the temperature range of 1073–1273 K in nitrogen or air medium. X-ray studies of the various compositions prepared in nitrogen medium revealed the following: (a) up to 7.5 mol% MnO, only the diffraction lines due to TeO_2 were detectable, (b) between 7.5 and 12.5 mol% MnO, $MnTe_6O_{13}$ was found to co-exist with TeO_2, (c) above 14.4 mol% MnO, lines due to $MnTe_6O_{13}$ and $MnTe_2O_5$ were seen, (d) in the range of ∼22.0–33.0 mol% MnO, $MnTe_2O_5$ was the main crystalline phase, (e) in the 35–40 mol% MnO range, $Mn_2Te_3O_8$, and $MnTe_2O_5$ were present together, and (f) beyond 45 and up to 50 mol% MnO, $MnTeO_3$ phase was present. The samples prepared in air medium were also reported to have yielded nearly identical results.

Based on DTA results, Ivanova [19] constructed a phase diagram of the MnO–TeO_2 binary system in the composition range of 0–50 mol% MnO. The phase diagram shows an eutectic between TeO_2 and $MnTe_6O_{13}$ at a composition of ≈9 mol% MnO and $T = 913$ K, an incongruent melting of $MnTe_6O_{13}$ at 923 K, an incongruent melting of $MnTe_2O_5$ at 973 K, a congruent melting of $Mn_2Te_3O_8$ at 993 K, and an eutectic between $Mn_2Te_3O_8$ and $MnTeO_3$ at a composition of ≈45 mol% MnO and $T \approx 950$ K.

Gospodinov and Mihov [20] prepared the phases $MnTeO_3$, $Mn_2Te_3O_8$, and $MnTe_2O_5$ by taking mixtures of $MnCO_3$(s) and TeO_2(s) in appropriate amounts on a platinum plate and heating in an inert medium in the temperature range of 950–975 K, for 3–6 h in two cycles. They measured the heat capacities of these phases in the temperature range of 400–560 K (by using a differential scanning calorimeter), and deduced the thermodynamic functions in the temperature range of 298.15–700 K.

To our knowledge, no report of the Mn–Te–O ternary phase diagram indicating the phase regions exists in literature.

2. Experimental

2.1. Sample preparation

Starting materials used for the preparation of different samples were: MnO(s) (Aldrich Inc., USA, purity: 99.99%), TeO_2(s) (Leico Industries Inc., USA, purity: 99.99%), $MnCO_3$(s) (Aldrich Inc., USA, purity: 99.9%) and Mn(s) (Leico Industries Inc., USA, purity: 99.9%). Thoroughly ground and homogenized mixtures of the starting materials were made into pellets of 10 mm diameter and placed in a platinum crucible or boat and heated. Four methods of preparation were employed.

2.1.1. Method 1 (under static argon atmosphere)

In this method, the platinum crucible was placed inside an SS tube (length 320 mm and diameter 45 mm), provided with gas inlet and outlet tubes, and closed using an SS lid with a copper gasket seal. The SS tube was flushed three or four times with argon gas, and ultimately filled with it. Samples were heated in two cycles. In the first cycle, the pellets were heated at 875 K for 15–20 h. After being cooled to room temperature, they were taken out, repelletized, and heated at 950–975 K for 15–20 h in the second cycle.

2.1.2. Method 2 (under vacuum sealed condition)

The platinum boat containing the sample pellets was placed inside a quartz tube of length 80–100 mm and diameter 15 mm, alternately flushed with argon and evacuated (three or four times), before being sealed under a vacuum of 10^{-6} Torr. The vacuum-sealed quartz tubes were heated at 875 K for 24 h, and at 950 K for ∼60 h.

2.1.3. Method 3 (under flowing argon/hydrogen)

The platinum boat containing the sample pellets was placed inside a long horizontal quartz tube of diameter 35 mm, the inlet of which was connected to the argon or hydrogen gas cylinder through a dehydrating medium, and the outlet led into water kept inside a beaker (for experiments involving argon) or onto a heated filament (for experiments involving hydrogen). Samples were heated under flowing argon or hydrogen at 875 K for 8–10 h, and at 950 K for 15–20 h.

2.1.4. Method 4 (in open air)

The pellets contained in the platinum boat were kept at the center of the mullite tube of an horizontal furnace, and heated at 950 K for 20–24 h in open air.

Two series of samples were prepared. In series 1, the samples were prepared solely from commercially obtained MnO and TeO_2 powders and by employing methods 1 and 2. In series 2, a variety of samples were prepared, and also with different set of starting materials. For instance, Mn_3O_4 was prepared by heating commercial MnO in air at 1275 K (method 4); Mn_3TeO_6 phase was prepared by heating commercial MnO and TeO_2 in air at 950 K (3:1 proportion; method 4); and MnO phase was freshly prepared by decomposing $MnCO_3$ in flowing hydrogen (method 3). Other starting materials such as (Mn+MnO+TeO_2), ($MnCO_3$+TeO_2), and (MnO, prepared from $MnCO_3$ + TeO_2) were also employed in this series.

Each sample was given an identification number in the sequence of its preparation with a prefix “BS” to mean “bulk sample”. All samples were phase characterized by X-ray powder diffraction patterns. The XRD patterns were recorded employing Cu Kα radiation (1.54 Å) using a Siemens D500 Diffractometer.

2.2. Mass spectrometric studies

A VG micromass mass spectrometer (MM 30 BK) was employed for vaporization studies. It consists of a Knudsen cell furnace assembly which permits effusion of equilibrium vapor, an electron impact ionization source where the gaseous species are ionized, a 90° sector single focusing magnetic analyzer (with a radius of curvature of 305 mm) for mass analysis of the positive ions, and a secondary electron multiplier/Faraday cup for ion detection. Alumina Knudsen cells with platinum liner were used in the present study. The Knudsen cell had the dimensions; i.d.: 7.5 mm, o.d.: 10.0 mm, height: 10.0 mm, and orifice (knife edged) diameter: 0.5 mm. It was placed inside a molybdenum cup having a removable but tightly fitting lid made of tungsten with a 3 mm diameter hole collinear with the Knudsen cell orifice. This assembly was heated by means of electron bombardment from two encircling tungsten filaments. Temperatures were measured by a chromel-to-alumel thermocouple, inserted through the base of the molybdenum cup and calibrated against the melting temperature of silver. With excellent temperature control, permitted by 'thermocouple control mode' of heating, the temperature measurement was accurate within ±3 K.

The mass spectra of the equilibrium vapor over all the samples consisted of peaks due to Te^+, Te_2^+, TeO^+, TeO_2^+, and O_2^+. The neutral species were ascertained to be Te_2(g), TeO(g), TeO_2(g), and O_2(g). The ion Te^+ was found to be a fragment ion having the origin mainly from TeO(g) [21]. Because of high background at the mass where the ion O_2^+ was detected, the measured ion intensities of O_2^+ were not considered reliable, and hence not used in further evaluation.

The general procedure was to heat the samples isothermally at 950 K and monitor the intensities of Te^+, Te_2^+, TeO^+, TeO_2^+, and O_2^+ ions as a function of time at an electron energy of 37.3 eV, and terminate the experiments when the intensities remained constant. As the samples were heated from room temperature, Te_2^+ and TeO_2^+ were also monitored.

A fresh aliquot of sample was used for each experiment. Two types of vaporization experiments were carried out: (i) experiments with aliquots of as-prepared samples and (ii) experiments after adding known excess of MnO to aliquots of some of the bulk samples. The samples, both before and after the vaporization experiments, were analyzed by XRD to identify the co-existing phases.

3. Results and discussion

The phases present in each sample were identified from the XRD patterns by comparing them with those of the Mn–Te–O ternary phases and of the starting materials, indexed in the JCPDS files [22]. The JCPDS indexing numbers used for comparison are given below: Mn(s) (32–637), MnO(s) (7–230), Mn_3O_4(s) (24–734), $MnCO_3$(s) (44–1472), Te(s) (36–1452), TeO_2(s) (9–433 or 42–1365), MnTe(s) (18–814), $MnTe_2$(s) (18–813), $MnTeO_3$(s) (24–744), Mn_3TeO_6(s) (21–1265), $Mn_2Te_3O_8$ (24–740), $MnTe_2O_5$ (30–828), and $Mn_6Te_5O_{16}$(s) (39–205).

3.1. Series 1 samples

Table 1 lists the starting compositions, methods of preparation, and the co-existing phases corresponding to the samples prepared with the starting materials MnO and TeO_2. The relative amounts of these two oxides were taken such that the samples would lie on the MnO(s) rich side of MnO–TeO_2 pseudo binary line. On the basis of information that at a composition of ~45 mol% MnO, an eutectic reaction occurs at ≈950 K and that $Mn_2Te_3O_8$(s) melts at 993 K [19], all our sample preparations (except sample 1) were restricted to heating at $T \leq 950$ K. As can be seen from Table 1, no sample, independent of the method of preparation, contained phases that lie exclusively on the MnO–TeO_2 binary line. All samples contained in addition to $MnTeO_3$, the ternary phase Mn_3TeO_6(s), which lies outside the MnO–TeO_2 binary line and in the oxygen-rich side of it. Furthermore, all (with the exception of BS#1) contained a third phase also, either $Mn_2Te_3O_8$(s) or Mn_3O_4.

That some unknown source of 'excess oxygen' caused the unintended formation of Mn_3TeO_6 or Mn_3O_4 phases

Table 1
Details of samples prepared in series 1

Method	Bulk sample no.	Initial composition[a]		Co-existing phases
		MnO (mol%)	$Mn_xTe_yO_z$	
1: Static argon	1	50.0	$Mn_{0.20}Te_{0.20}O_{0.60}$	$MnTeO_3 + Mn_3TeO_6$ (traces)
	2	57.1	$Mn_{0.23}Te_{0.18}O_{0.59}$	$MnTeO_3 + Mn_3TeO_6 + Mn_2Te_3O_8$
	3	66.7	$Mn_{0.29}Te_{0.14}O_{0.57}$	$MnTeO_3 + Mn_3TeO_6 + Mn_2Te_3O_8$
2: Vacuum sealed	4	50.0	$Mn_{0.20}Te_{0.20}O_{0.60}$	$MnTeO_3 + Mn_3TeO_6 + Mn_2Te_3O_8$
	19	50.0	$Mn_{0.20}Te_{0.20}O_{0.60}$	$MnTeO_3 + Mn_3TeO_6 + Mn_2Te_3O_8$
	5	53.5	$Mn_{0.22}Te_{0.19}O_{0.59}$	$MnTeO_3 + Mn_3TeO_6 + Mn_2Te_3O_8$
	6	78.8	$Mn_{0.36}Te_{0.10}O_{0.54}$	$MnTeO_3 + Mn_3O_4 + Mn_3TeO_6$ (traces)

The starting materials were commercially obtained MnO and TeO_2. Temperature of preparation was 950 K except for sample 1 for which $T = 975$ K.

[a] The compositions were deduced from the initial mass of MnO and TeO_2 taken for preparation.

Table 2
Details of samples prepared in series 2

Method	Starting compounds	Bulk sample no.	Phases identified
4: Heating in air	$3MnO + 1TeO_2$	7[a]	Mn_3TeO_6
	$3MnO + 1TeO_2$	24[a]	$Mn_3TeO_6 + TeO_2$
	MnO	20[b]	Mn_3O_4
	MnO	25[b]	Mn_3O_4
	MnO	26[b]	Mn_3O_4
3: In flowing hydrogen	$MnCO_3$	21[a]	MnO
	$MnCO_3$	22[a]	MnO

The starting materials were commercially obtained.
[a] Temperature of preparation: 950 K.
[b] Temperature of preparation: 1275 K.

was supported by the results obtained on heating ($3MnO + 1TeO_2$) or MnO in air (see Table 2). Mn_3TeO_6 or Mn_3O_4 were the products.

The generation of Mn_3TeO_6 phase obviously indicates that the overall condensed phase compositions might be different from (slightly more O-rich relative to) the assumed initial compositions that are given in Table 1. The MnO(s) used in these preparations might have been of hyper-stoichiometric composition, thus forcing the samples to lie on the O-rich side of the $MnO–TeO_2$ line. Knowing the tendency of manganese monoxide phase to pick up oxygen up to $MnO_{1.13}$ without really generating a new phase [23], we did take care to always store the MnO powder in high purity argon atmosphere glove box. For the preparation of BS#19 sample, MnO from a freshly unsealed bottle was employed, but the result was similar to BS#4 preparation.

In the case of preparation by method 1, the oxygen-enrichment of the condensed phase might also have been caused by vapor transport to and deposition in the cooler part of the SS tube, should the vapor composition be of $Te/O > 0.5$, that is, should the loss of tellurium be greater than that with a volatilization loss as TeO_2. That the BS#1 sample, which was prepared at slightly higher temperature of 975 K, did not contain the third phase $Mn_2Te_3O_8$ supports this supposition—higher vapor pressure promoting the disappearance of the $Mn_2Te_3O_8$ phase.

Through preparation of series 1 samples, we could gain some insight into the phase diagram: that the phases $MnTeO_3$ and Mn_3TeO_6 would exist in equilibrium with each other; and also with $Mn_2Te_3O_8$ or Mn_3O_4 to form respective three-phase regions.

3.2. Vaporization studies with series 1 samples

3.2.1. Experiments with as-prepared samples

Some of the samples were subjected to isothermal vaporization at 950 K to identify the condensed phases in equilibrium with vapor under effusion conditions. The details pertaining to high temperature mass spectrometric experiments (numbered sequentially with a prefix "VS" to mean "vaporization study") including the duration of vaporization at 950 K and the phases present before and after the vaporization experiments are given in Table 3.

Fig. 1 shows the XRD patterns of BS#1 and of the residues obtained after subjecting different aliquots of BS#1 for vaporization experiments (VS#2–4) of increasing time durations at 950 K. As the duration of vaporization experiment increased, the intensity of peak due to the phase $MnTeO_3$ decreased and that due to the phase Mn_3TeO_6 increased, the change most pronounced for VS#4. Some common features of the isothermal vaporization experiments with BS#1 were: (1) the residues retained both the phases, $MnTeO_3$(s) and Mn_3TeO_6(s), which were present before vaporization, and (2) no third phase could be detected in the residues even when the experiment was conducted for duration as long as 2050 min (VS#5). Fig. 2 shows a plot of ion intensities of TeO_2^+, TeO^+, and Te_2^+, and also of the ratios of ion intensities TeO^+/TeO_2^+, and Te_2^+/TeO_2^+ as a function of time in the case of VS#5.

Table 3
Details pertaining to vaporization experiments with as-prepared series 1 samples

Experiment no. (VS#)	Bulk sample no.	Starting composition MnO (mol%)	Initial mass (g)	Mass loss (g)	Co-existing phases in the as-prepared samples	Duration of heating at 950 K (min)	Co-existing phases in the vaporization residue
2	1	50.0	0.06178	0.00242	$MnTeO_3 + Mn_3TeO_6$	360	$MnTeO_3 + Mn_3TeO_6$
3	1	50.0	0.06396	0.00283	$MnTeO_3 + Mn_3TeO_6$	680	$MnTeO_3 + Mn_3TeO_6$
4	1	50.0	0.05945	0.00610	$MnTeO_3 + Mn_3TeO_6$	1899	$MnTeO_3 + Mn_3TeO_6$
5	1	50.0	0.06431	0.00568	$MnTeO_3 + Mn_3TeO_6$	2049	$MnTeO_3 + Mn_3TeO_6$
6	2	57.1	0.06632	0.00179	$MnTeO_3 + Mn_3TeO_6 + Mn_2Te_3O_8$	384	$MnTeO_3 + Mn_3TeO_6$
7	3	66.7	0.05558	0.00202	$MnTeO_3 + Mn_3TeO_6 + Mn_2Te_3O_8$	453	$MnTeO_3 + Mn_3TeO_6$
8[a]	4	50.0	0.06473	0.00959	$MnTeO_3 + Mn_3TeO_6 + Mn_2Te_3O_8$	2045	$MnTeO_3 + Mn_3TeO_6$
9[a]	4	50.0	0.06556	0.01166	$MnTeO_3 + Mn_3TeO_6 + Mn_2Te_3O_8$	3280	$MnTeO_3 + Mn_3TeO_6$
10[a]	5	53.5	0.06552	0.00611	$MnTeO_3 + Mn_3TeO_6 + Mn_2Te_3O_8$	2041	$MnTeO_3 + Mn_3TeO_6$
11[a]	5	53.5	0.03193	0.00950	$MnTeO_3 + Mn_3TeO_6 + Mn_2Te_3O_8$	1987	$MnTeO_3 + Mn_3TeO_6$
12	6	78.7	0.06376	0.00158	$MnTeO_3 + Mn_3O_4 + Mn_3TeO_6$	484	$MnTeO_3 + Mn_3O_4 + Mn_3TeO_6$
13	6	78.7	0.03300	0.00218	$MnTeO_3 + Mn_3O_4 + Mn_3TeO_6$	752	$Mn_3O_4 + Mn_3TeO_6$
14	6	78.7	0.07376	0.00077	$MnTeO_3 + Mn_3O_4 + Mn_3TeO_6$	206	$MnTeO_3 + Mn_3O_4 + Mn_3TeO_6$

[a] The estimated final condensed phase compositions: $O/(Mn + Te) = 1.5$ and $O/Te = 3.4$ (VS#8), 3.5 (VS#9), 3.5 (VS#10) and 4.8 (VS#11).

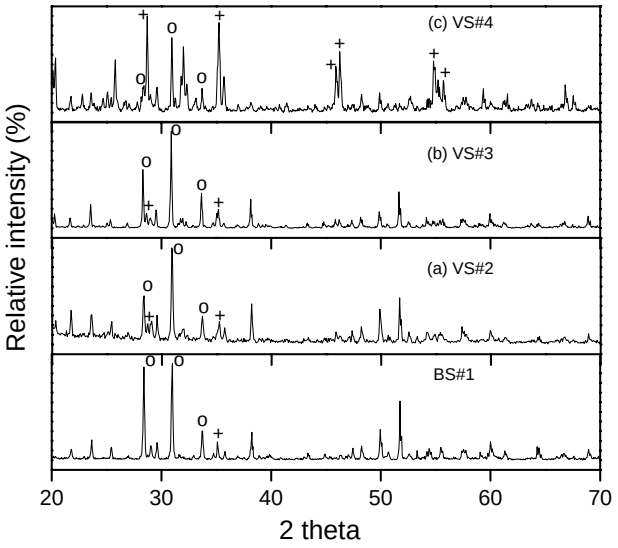

Fig. 1. Comparison of XRD of BS#1 before and after vaporization experiments. (a) After heating for 360 min (VS#2), (b) after heating for 680 min (VS#3), and (c) after heating for 1899 min (VS#4). (+) Major intensity peaks of Mn_3TeO_6, and (○) major intensity peaks for $MnTeO_3$.

The XRD patterns of the residues of the vaporization experiments (VS#6–11) conducted by employing the samples BS#2–5 have also indicated the presence of only two phases, namely $MnTeO_3$ and Mn_3TeO_6. Fig. 3 shows, for example, the XRD patterns corresponding to BS#3 and the residue of VS#7. The third phase $Mn_2Te_3O_8$ that was present in the samples (BS#2–5) had obviously disappeared during vaporization. Even when subjected to continuous vaporization for long time (up to ∼3300 min; VS#8–11), the residues showed the presence of only $MnTeO_3$(s) and Mn_3TeO_6(s). No third phase, a binary (Mn + O) or a ternary (Mn + Te + O) could be detected.

Three vaporization experiments were conducted with BS#6. When the duration of the experiment was short (206 min in VS#14, and 484 min in VS#12), the ion intensities remained constant and the XRD patterns of the residues indicated the retention of the same three phases (namely Mn_3TeO_6, $MnTeO_3$, and Mn_3O_4) that were originally present. In the other experiment (VS#13), the duration was higher (752 min), and the ion intensities after remaining constant for some time, started to decrease. The XRD pattern of the residue of this experiment indicated the presence of only two phases namely Mn_3TeO_6 and Mn_3O_4. In Fig. 4, XRD patterns of the bulk sample (BS#6) and those of vaporization residues (of VS#12–14) are compared.

3.2.2. Experiments after adding a known excess of MnO

Known amounts of MnO(s) were added to aliquots of some bulk samples to obtain an initial $x(MnO) = 0.8$ (with BS#1–3) and $x(MnO) = 0.9$ (with BS#6). The residues from all vaporization experiments with such samples showed a new phase Mn_3O_4. The co-existing phase was Mn_3TeO_6 in experiments VS#18–22, while it was MnO in experiments VS#23 and VS#24. The $Mn_2Te_3O_8$ phase and even the $MnTeO_3$ phase disappeared during vaporization leaving

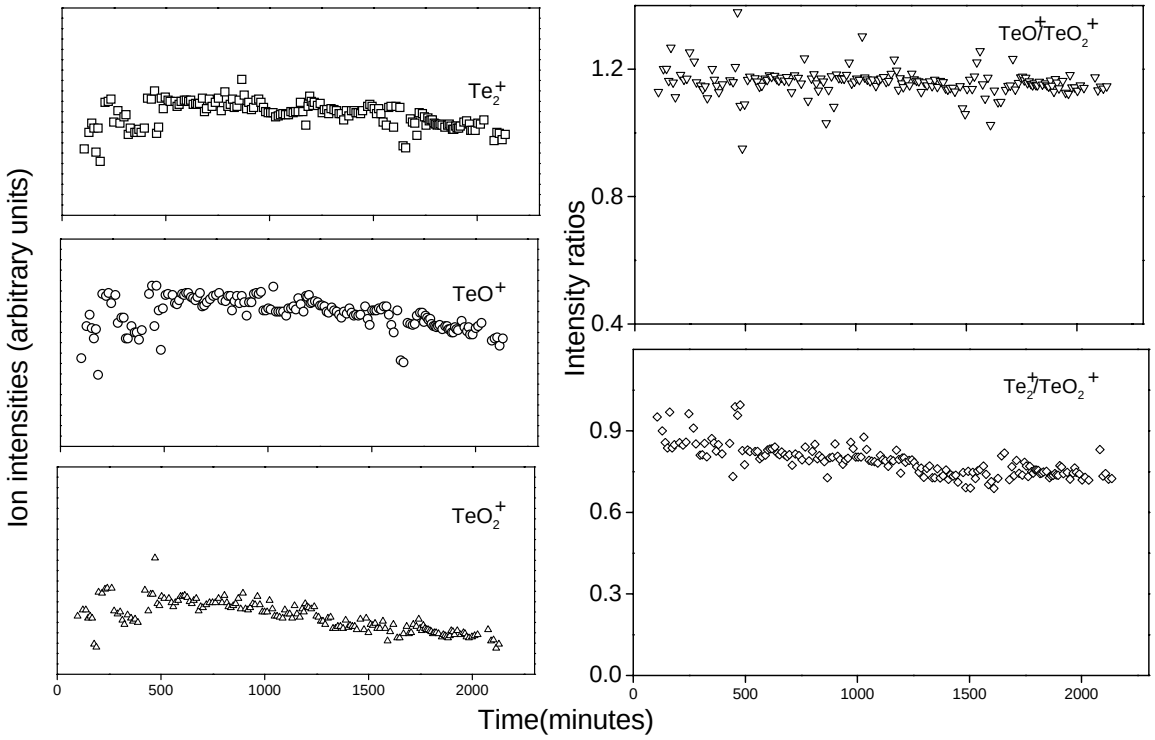

Fig. 2. Ion intensities and their ratios as a function of time during the vaporization experiment of VS#5. Starting sample: BS#1; composition: $Mn_{0.2}Te_{0.2}O_{0.6}$, prepared under static argon condition at 975 K. Phases present in the bulk sample and after the vaporization experiment: $MnTeO_3(s) + Mn_3TeO_6(s)$.

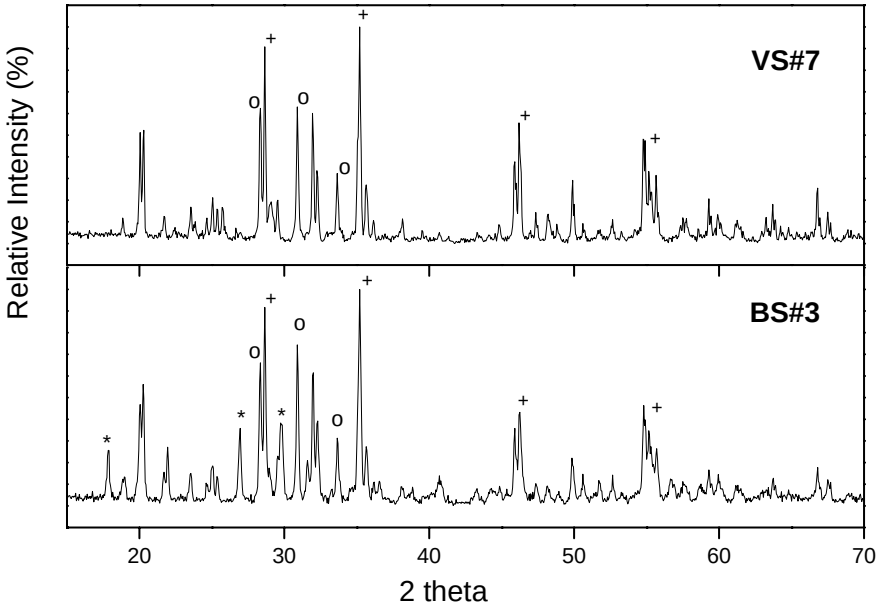

Fig. 3. XRD of BS#3 (66.7 mol% MnO: static argon) before and after vaporization experiment (VS#7). (∗) Major peaks due to $Mn_2Te_3O_8$, (○) major peaks due to $MnTeO_3$, and (+) major peaks due to Mn_3TeO_6.

no ternary phase of the MnO–TeO_2 binary line. The details pertaining to these vaporization experiments are given in Table 4.

In VS#23 and VS#24 experiments, which had an overall initial composition of ∼90 mol% MnO, no measurable intensities for TeO^+ and $TeO_2{}^+$ were observed. Initially, the $I(Te_2{}^+)$ was measurable, but it decreased fast to immeasurably low values towards the end of the experiment, consistent with the XRD of the residues which showed the presence of only Mn_3O_4 and MnO phases.

There occurred a significant evolution of tellurium in these experiments as the samples were slowly heated from room temperature to reach 950 K. The $I(Te_2{}^+)$ at 800 K < T < 950 K was approximately two orders of magnitude higher than that observed in experiments with as-prepared samples (VS#2–14) at similar temperatures. Upon attainment of T = 950 K, the $I(Te_2{}^+)$ decreased to stable values, comparable to those observed in VS#2–14.

In addition to revealing the general tendency of the system to force the condensed phase compositions move away from the MnO–TeO_2 binary line, the vaporization experiments with series 1 samples (as prepared and with known excess of MnO) provided support for the existence of equilibrium between the phases $MnTeO_3$ and Mn_3TeO_6, as well as between the phases Mn_3O_4 and Mn_3TeO_6.

3.3. Series 2 samples

3.3.1. Samples prepared with Mn(s) as one of the starting materials

From the above discussion pertaining to the preparation of series 1 samples or to the experiments with them,

Table 4
Details of vaporization experiments conducted by adding known amounts of MnO to aliquots from series 1 samples

Experiment no. (VS#)	Bulk sample no.	Bulk sample composition MnO (mol%)	Composition after the MnO addition MnO (mol%)	Initial mass (g)	Mass loss (g)	Duration of heating at 950 K (min)	Phases present	
							In the starting sample	In the vaporization residue
18	1	50.0	79.0	0.06128	0.00248	510	($MnTeO_3$ + Mn_3TeO_6) + MnO	Mn_3O_4 + Mn_3TeO_6
19	1	50.0	80.2	0.05416	0.00452	1642	($MnTeO_3$ + Mn_3TeO_6) + MnO	Mn_3O_4 + Mn_3TeO_6
20	3	66.7	80.0	0.05571	0.00161	411	($MnTeO_3$ + Mn_3TeO_6 + $Mn_2Te_3O_8$) + MnO	Mn_3O_4 + Mn_3TeO_6
21	3	66.7	80.0	0.06060	0.00218	779	($MnTeO_3$ + Mn_3TeO_6 + $Mn_2Te_3O_8$) + MnO	Mn_3O_4 + Mn_3TeO_6
22	2	57.1	80.1	0.08275	0.00376	697	($MnTeO_3$ + Mn_3TeO_6 + $Mn_2Te_3O_8$) + MnO	Mn_3O_4 + Mn_3TeO_6
23	6	78.7	90.0	0.06479	0.00123	417	($MnTeO_3$ + Mn_3O_4 + Mn_3TeO_6) + MnO	Mn_3O_4 + MnO
24	6	78.7	90.0	0.06195	0.00088	387	($MnTeO_3$ + Mn_3O_4 + Mn_3TeO_6) + MnO	Mn_3O_4 + MnO

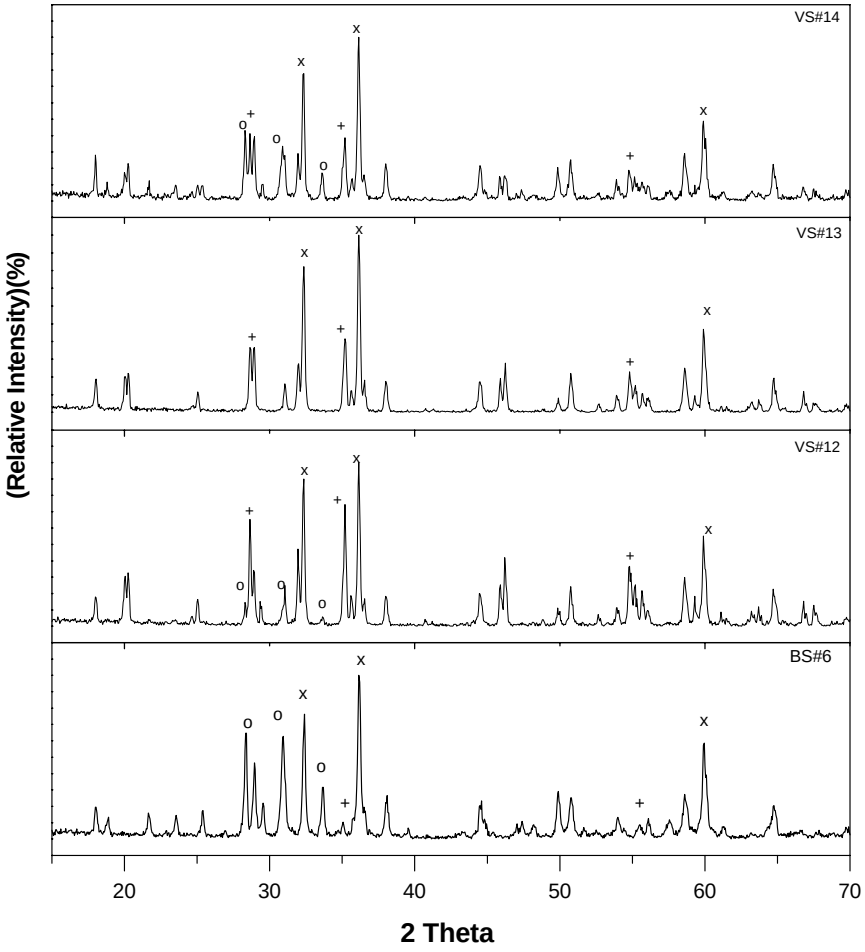

Fig. 4. Comparison of XRD of BS#6 (78.7 mol% MnO) and residues of VS#12–14. (+) Major peaks due to Mn_3TeO_6, (○) major peaks due to $MnTeO_3$, and (×) major peaks due to Mn_3O_4. When the duration of the vaporization experiment was less (206 min in VS#14, and 484 min in VS#12) the phases originally present were retained, with intensity due to $MnTeO_3$(s) relatively decreased. When the duration was increased to 752 min (VS#13), peaks due to the phase $MnTeO_3$(s) disappeared.

it is evident that we did not succeed in having MnO to co-exist with a ternary phase, even when $x(\mathrm{MnO}) > 0.55$. Supposing that this situation arose because the overall initial compositions were or became (during preparation or vaporization) oxygen-rich relative to the intended initial compositions, preparation with an initial composition below the $MnO–TeO_2$ binary line was attempted in series 2. Solid manganese was used as one of the starting materials along with MnO(s) and TeO_2(s) to achieve this, and to restore the stoichiometry of MnO phase to that controlled by Mn(s)–MnO(s) equilibrium. Preparation under flowing argon conditions was employed to make the overall sample composition move towards or cross the $MnO–TeO_2$ binary line. Three samples (BS#8–10) were prepared in this way, and the details are given in Table 5. The XRD of all these samples showed ($MnO + Mn_6Te_5O_{16} + Mn_3O_4$). This was the first time that we could succeed in having MnO(s) to co-exist with a tellurite phase, and in having the phase $Mn_6Te_5O_{16}$(s) prepared. Identification of Mn_3O_4(s) as the third phase shows that the sample did move across the $MnO–TeO_2$ binary line. This fact together with the observation of black deposits on the cooler parts of the quartz tube led us to infer that there was a large preferential evolution of tellurium during the solid state reaction that eventually gave rise to the three phase mixture ($MnO + Mn_6Te_5O_{16} + Mn_3O_4$).

Another preparation (BS#27) that involved a mixture of Mn, MnO, and TeO_2 (but with so large amount of Mn that the overall apparent initial composition was $Mn_{0.60}Te_{0.05}O_{0.35}$) resulted in yielding a three phase mixture of Mn + MnO + MnTe.

3.3.2. *Samples prepared with ($TeO_2 + MnCO_3$) or (TeO_2 + MnO, prepared from $MnCO_3$) as starting materials*

The next set of preparations were attempted using the freshly prepared MnO (by decomposing $MnCO_3$ under flowing hydrogen conditions). Since, the MnO phase derived from carbonate at $T \geq 775$ K is likely to be less active in taking up oxygen than that prepared at low temperatures [23], use of this MnO might serve better to prepare Mn–Te–O samples along the $MnO–TeO_2$ binary line than that of the commercially obtained MnO samples, especially

Table 5
Details of samples prepared in series 2

Method	Starting materials	Bulk sample no.	Starting composition	Co-existing phases
3: Flowing argon	Mn, MnO[a], TeO_2	8	$Mn_{0.35}Te_{0.16}O_{0.49}$	$MnO + Mn_6Te_5O_{16} + Mn_3O_4$
	Mn, MnO[a], TeO_2	9	$Mn_{0.34}Te_{0.17}O_{0.49}$	$MnO + Mn_6Te_5O_{16} + Mn_3O_4$
	Mn, MnO[a], TeO_2	10	$Mn_{0.35}Te_{0.16}O_{0.49}$	$MnO + Mn_6Te_5O_{16} + Mn_3O_4$
	$MnCO_3$, TeO_2	14[b]	$Mn_{0.20}Te_{0.20}O_{0.60}$	$MnTeO_3 + Mn_3TeO_6 + Mn_2Te_3O_8$
	$MnCO_3$, TeO_2	17[c]	$Mn_{0.17}Te_{0.22}O_{0.61}$	$MnTeO_3 + Mn_3TeO_6 + Mn_2Te_3O_8$
	$MnCO_3$, TeO_2	13[d]	$Mn_{0.36}Te_{0.10}O_{0.54}$	$MnTeO_3 + Mn_3TeO_6 + Mn_3O_4$
	$MnCO_3$, TeO_2	18[e]	$Mn_{0.14}Te_{0.24}O_{0.62}$	$Mn_2Te_3O_8 + MnTe_2O_5$
2: Vacuum seal	MnO[f], TeO_2	12[d]	$Mn_{0.36}Te_{0.10}O_{0.54}$	$MnTeO_3 + Mn_6Te_5O_{16} + Mn_3O_4$
	Mn, MnO[a],TeO_2	27	$Mn_{0.60}Te_{0.05}O_{0.35}$	Mn + MnO + MnTe

Temperature of preparation for all samples: 950 K.
[a] Commercially obtained MnO(s) was used.
[b] Corresponds to 50.3 mol% MnO.
[c] Corresponds to 42.8 mol% MnO.
[d] Corresponds to 78.7 mol% MnO.
[e] Corresponds to 37.1 mol% MnO.
[f] MnO(s) obtained from $MnCO_3$(s) was used.

when vacuum-seal method is employed. In preparations under flowing argon, use of $MnCO_3$(s) would generate MnO(s) in situ, and thus is of even greater advantage.

Table 5 lists the samples prepared with $MnCO_3$(s) or MnO(s) obtained from it as one of the starting materials. The effective MnO% in the samples when $MnCO_3$(s) and TeO_2(s) were employed are: 78.7 (BS#13), 50.3 (BS#14), 42.8 (BS#17), and 37.1 (BS#18). The last two compositions were chosen to examine whether the phase Mn_3TeO_6 is formed even when MnO mol% is <50. The phase characterization of BS#14 and BS#17 revealed that they both contained the Mn_3TeO_6 phase, apart from the phases $MnTeO_3$(s) and $Mn_2Te_3O_8$(s). The BS#13 sample also contained the Mn_3TeO_6 phase, but along with $MnTeO_3$ and Mn_3O_4. The BS#18 contained only two phases $Mn_2Te_3O_8 + MnTe_2O_5$, both lying solely on MnO–TeO_2 binary line, thus becoming the only sample, preparation of which was in accord with the intended starting composition.

The only three-phase region that remains to be unambiguously confirmed on the MnO-rich side is ($Mn_3O_4 + Mn_6Te_5O_{16} + MnTeO_3$). The ambiguity arose with an examination of BS#6, BS#12, and BS#13 samples, all having identical starting composition of ≈78.7 mol% MnO, but only BS#12 yielding the above three-phase mixture whereas BS#6 and BS#13 yielded another three-phase mixture ($Mn_3O_4 + Mn_3TeO_6 + MnTeO_3$). With regard to the phases outside the MnO–TeO_2 binary line, BS#12 contained one (Mn_3O_4), while BS#6 and BS#13 contained two (Mn_3O_4 and Mn_3TeO_6). Possible difference in the stoichiometry of MnO used in BS#6 and BS#12 (both vacuum seal) and the vapor transport in BS#13 (under flowing-argon) might have contributed to obtain above results.

The XRD patterns of different three-phase regions identified are compared in Fig. 5 along with that of Mn_3TeO_6 phase.

Preparation of the series 2 samples led to the identification of existence of two three-phase regions involving $Mn_6Te_5O_{16}$: (1) with MnO and Mn_3O_4; and (2) with Mn_3O_4 and $MnTeO_3$. It also led to confirm the equilibrium between $Mn_2Te_3O_8$ and $MnTe_2O_5$.

3.4. Further phase equilibration studies

To confirm the existence of some of the above mentioned phase regions, some more phase equilibration studies were conducted with Mn_3TeO_6 as one of the starting materials, and the details are given in Table 6. With Mn, MnO, and Mn_3TeO_6 as the starting materials, and an overall composition above the MnO–TeO_2 binary line, BS#11 was prepared under vacuum-sealed conditions. This preparation yielded the same three phase mixture as did BS#8 to BS#10, namely ($MnO + Mn_3O_4 + Mn_6Te_5O_{16}$).

To further confirm that the two binary oxides of manganese (MnO and Mn_3O_4) can co-exist only with $Mn_6Te_5O_{16}$ and not with either $MnTeO_3$ or Mn_3TeO_6, preparations were carried out using vacuum seal method with: (1) MnO, Mn_3TeO_6, and Mn_3O_4 as the starting materials (BS#15)— to examine whether Mn_3TeO_6 remains after heating; and (2) ($2MnO + Mn_3TeO_6$) as the starting materials (BS#16)—to examine whether a reaction such as

$$MnO(s) + Mn_3TeO_6(s) = Mn_3O_4(s) + MnTeO_3(s) \quad (2)$$

might result in the formation of ($MnO + Mn_3O_4 + MnTeO_3$).

Both preparations resulted in the disappearance of MnO(s) and formation of ($Mn_3O_4 + Mn_3TeO_6$) as the end co-existing phases. The XRD pattern of the BS#15 indicated the presence of ($MnTeO_3 + Mn_3TeO_6 + Mn_3O_4$) at the end of the first cycle, but, on further heating in the second cycle, the phase $MnTeO_3$ disappeared to yield ($Mn_3TeO_6 + Mn_3O_4$). These experiments also served to support our earlier inference that Mn(s) would need to be used in preparation to be able to retain MnO(s) and a tellurite phase together.

Combining all the results given above, we deduce that the following three-phase regions exist under equilibrium

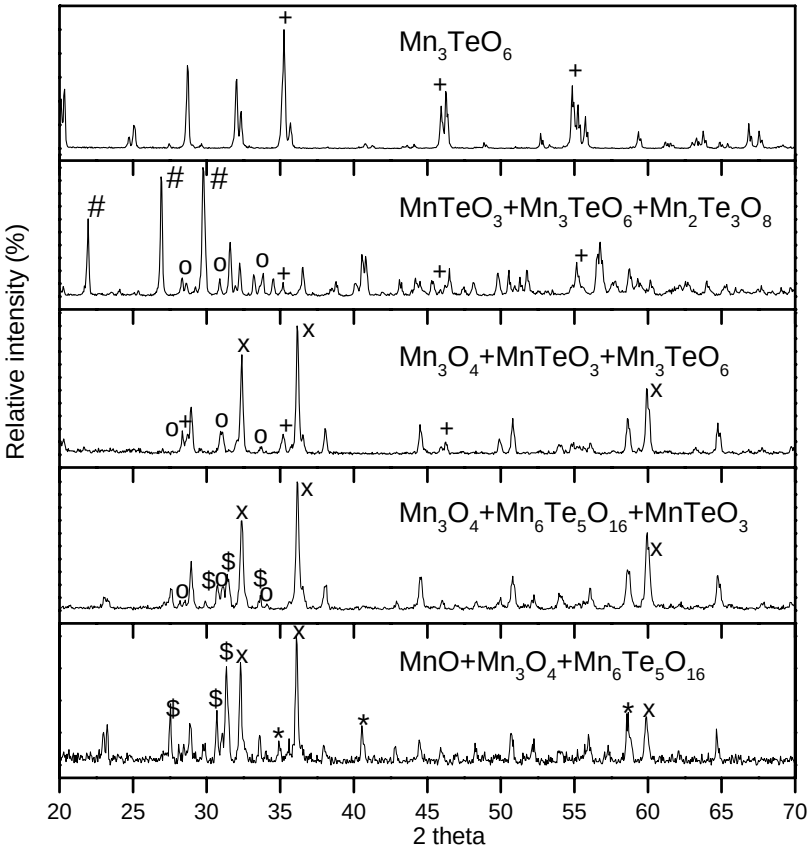

Fig. 5. XRD patterns of the four three-phase regions identified in this study along with that of the single phase Mn_3TeO_6(s), prepared in BS#7. $MnO + Mn_3O_4 + Mn_6Te_5O_{16}$: phase region 1, $Mn_3O_4 + Mn_6Te_5O_{16} + MnTeO_3$: phase region 2, $Mn_3O_4 + MnTeO_3 + Mn_3TeO_6$: phase region 3, and $MnTeO_3 + Mn_2Te_3O_8 + Mn_3TeO_6$: phase region 4. The most intense peaks of each phase are marked: (∗) MnO, (×) Mn_3O_4, ($) $Mn_6Te_5O_{16}$, (○) $MnTeO_3$, (+) Mn_3TeO_6, and (#) $Mn_2Te_3O_8$.

conditions at 950 K: $MnO + Mn_3O_4 + Mn_6Te_5O_{16}$ (phase region 1; PH1), $Mn_3O_4 + Mn_6Te_5O_{16} + MnTeO_3$ (phase region 2; PH2), $Mn_3O_4 + MnTeO_3 + Mn_3TeO_6$ (phase region 3; PH3) and $MnTeO_3 + Mn_2Te_3O_8 + Mn_3TeO_6$ (phase region 4; PH4).

3.5. Vaporization studies on three-phase regions

Conclusive evidence for the existence of above mentioned four three-phase regions was sought to be obtained by conducting isothermal vaporization experiments with aliquots of BS#9, BS#12, BS#13, and BS#17. At 950 K, the ion intensities (proportional to partial pressures at a given temperature) remained invariant as a function of time. The XRD patterns of the vaporization residues showed retention of the same phases originally present. These results together with the application of phase rule, served to confirm of PH1, PH2, PH3, and PH4. Table 7 gives the details.

3.6. Phase diagram of Mn–Te–O

Based on the results given above, a phase diagram of Mn–Te–O, around the $MnO–TeO_2$ line at 950 K was constructed and is given in Fig. 6. An enlarged portion, comprising the composition range lying within $MnO–TeO_2–Mn_3O_4$, is shown in Fig. 7.

Table 6
Details of the phase equilibration studies carried out to confirm the ternary phases which could co-exist with MnO and/or Mn_3O_4

Bulk sample no.	Starting composition	Starting materials	Co-existing phases after the heating
11[a]	$Mn_{0.39}Te_{0.06}O_{0.55}$	Mn, MnO, Mn_3TeO_6	$MnO + Mn_6Te_5O_{16} + Mn_3O_4$
15[b]	$Mn_{0.37}Te_{0.05}O_{0.58}$	MnO, Mn_3O_4, Mn_3TeO_6	$MnTeO_3 + Mn_3TeO_6 + Mn_3O_4$ (Cycle 1) $Mn_3TeO_6 + Mn_3O_4$ (Cycle 2)
16[a]	$Mn_{0.36}Te_{0.07}O_{0.57}$	MnO, Mn_3TeO_6	$Mn_3TeO_6 + Mn_3O_4$

Temperature of preparation: 950 K; method of preparation: vacuum seal (method 2).
[a] Commercially obtained MnO was used.
[b] MnO obtained from $MnCO_3$ was used.

Table 7
Details of isothermal vaporization experiments conducted with series 2 samples to confirm the four three-phase regions identified

Experiment no. (VS#)	Bulk sample no.	Initial mass (g)	Mass loss (g)	Co-existing phases of the starting sample	Duration of heating[a] at 950 K (min)	Co-existing phases in the residues of vaporization experiments
27	9	0.06693	0.00065	$MnO + Mn_6Te_5O_{16} + Mn_3O_4$	~300	$MnO + Mn_6Te_5O_{16} + Mn_3O_4$
28	12	0.05923	0.00124	$Mn_3O_4 + Mn_6Te_5O_{16} + MnTeO_3$	~700	$Mn_3O_4 + Mn_6Te_5O_{16} + MnTeO_3$
29	13	0.05301	0.00049	$MnTeO_3 + Mn_3TeO_6 + Mn_3O_4$	~240	$MnTeO_3 + Mn_3TeO_6 + Mn_3O_4$
30	17	0.07782	0.00762	$MnTeO_3 + Mn_3TeO_6 + Mn_2Te_3O_8$	~240	$MnTeO_3 + Mn_3TeO_6 + Mn_2Te_3O_8$

[a] The samples were also subjected to isothermal vaporization at $T < 950$ K for varying durations.

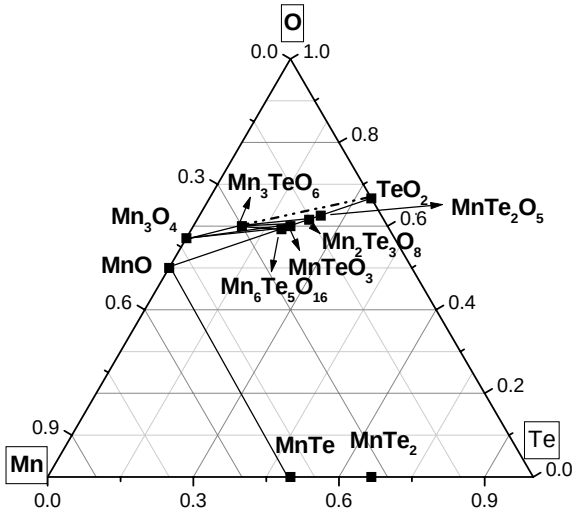

Fig. 6. Mn–Te–O phase diagram at 950 K. The narrow three-phase regions ($Mn_3O_4 + Mn_6Te_5O_{16} + MnTeO_3$), ($Mn_3O_4 + MnTeO_3 + Mn_3TeO_6$), and ($MnTeO_3 + Mn_3TeO_6 + Mn_2Te_3O_8$) can be seen more clearly in Fig. 7.

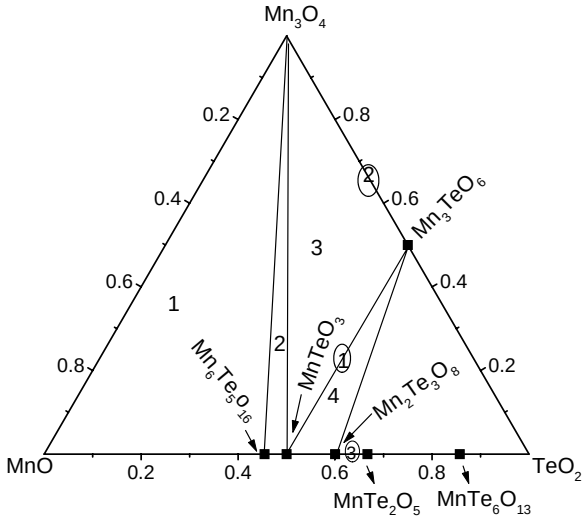

Fig. 7. Enlarged portion (comprising the composition range lying within $MnO–TeO_2–Mn_3O_4$) of the Mn–Te–O phase diagram at 950 K. The numbers 1, 2, 3, and 4 indicate the three-phase regions identified in this study. The circled numbers refer to the two-phase regions observed in this study.

While the existence of different phases in the Mn–Te–O system was known already [16–20], how they co-exist and the corresponding phase regions are being reported for the first time. We find $Mn_6Te_5O_{16}$ to co-exist with MnO and Mn_3O_4 at 950 K. This finding is not in accord with that reported by Trömel and coworkers [16,17], who hypothesized that disproportionation of $Mn_6Te_5O_{16}$, according to reaction 1, starts at 923 K itself, and that it would lead to the formation of $MnTeO_3$ and Mn_3TeO_6. Whether the presence of MnO and Mn_3O_4 could have altered the temperature range of stability of $Mn_6Te_5O_{16}$ or the way it would decompose is uncertain. Some of our results such as $Mn_6Te_5O_{16}$ and $Mn_2Te_3O_8$ being the phases present on either side of $MnTeO_3$ along the $MnO–TeO_2$ binary line, and generation of Mn_3TeO_6 in many preparations as well as its build up in many effusion experiments are in accord with Trömel and Schmid [16] observations: $MnTeO_3$ was formed when MnO and TeO_2 were taken in equal ratio of 1:1, Mn_3TeO_6 was formed when the MnO content was slightly more (1:0.9), and $Mn_2Te_3O_8$ was formed when TeO_2 was slightly more (0.9:1). While Trömel and Schmid [16] did not mention how Mn_3TeO_6 would co-exist with the phases along the $MnO–TeO_2$ binary line, the present study showed that it can co-exist with $MnTeO_3$ and $Mn_2Te_3O_8$ and not with $Mn_6Te_5O_{16}$.

The Mn_3TeO_6 phase was not identified by Ivanova [19] even when the preparations were performed in air medium and the compositions chosen were 47.5 mol% MnO. This was rather surprising to us because in the present study Mn_3TeO_6 was observed in many of our preparations. Bayer's [18] preparation of the compound Mn_3TeO_6 by heating MnO and TeO_2 in air was confirmed in the present study.

We could not prepare $MnTeO_3$ as single phase in our study, even though preparations using different starting compositions and different routes were made. This compound was prepared, apparently as a pure phase, by Gospodinov and Mihov [20], Ivanova [19], and Trömel and Schmid [16]. We do not know the reason for this discrepancy. Based on a number of preparations conducted in the present study, we believe that unless one can prevent all forms of oxygen enrichment of the condensed phase, $MnTeO_3$ co-existing with at least a small amount of Mn_3TeO_6 will be the result.

Apart from the existence of four three-phase regions, that of three two-phase regions such as ($Mn_3TeO_6 + MnTeO_3$), ($Mn_3O_4 + Mn_3TeO_6$), and ($Mn_2Te_3O_8 + MnTe_2O_5$) have

also been identified in the present study. The co-existence of ($Mn_2Te_3O_8$ + $MnTe_2O_5$) in the composition range of 35–40 mol%, MnO had been already reported by Ivanova [19]. In the case of (Mn_3TeO_6 + $MnTeO_3$), we had presented previously [14] the strong evidence for the existence of an univariant three-phase equilibrium (Mn_3TeO_6 + $MnTeO_3$ + vapor) in many mass spectrometric vaporization experiments. Though the (Mn_3O_4 + Mn_3TeO_6) two-phase region was also identified in the residues of many vaporization experiments as well as in the bulk samples, mass spectrometric results [14] did not support the existence of an univariant equilibrium of (Mn_3O_4 + Mn_3TeO_6 + vapor).

4. Conclusions

The present study began with the objective of identifying the phases on the MnO-rich side of the MnO–TeO_2 pseudo binary line. However, the X-ray diffraction investigations on the bulk samples and on the vaporization residues, as well as the vaporization behavior exhibited by the samples revealed the complexity of the system, and consequently, a vast number of preparations and vaporization experiments had to be undertaken to obtain a meaningful understanding of the results. A ternary phase diagram of the Mn–Te–O system, with an emphasis on the phases in and around the MnO–TeO_2 binary line, is presented for the first time.

Acknowledgements

We thank the X-ray group for carrying out X-ray diffraction analysis of several samples. Thanks are also due to the electronics group for the maintenance of the mass spectrometer. We thank Dr. G. Periaswami (Head, Materials Chemistry Division) and Dr. P.R. Vasudeva Rao (Head, Fuel Chemistry Division and Associate Director, Chemical Group) for their encouragement.

References

[1] T.S. Lakshmi Narasimhan, Ph.D. Thesis, University of Madras, 2000.
[2] B. Saha, R. Viswanathan, M. Sai Baba, D. Darwin Albert Raj, R. Balasubramanian, D. Karunasagar, C.K. Mathews, J. Nucl. Mater. 130 (1985) 316.
[3] M. Sai Baba, R. Viswanathan, R. Balasubramanian, D. Darwin Albert Raj, B. Saha, C.K. Mathews, J. Chem. Thermodyn. 20 (1988) 1157.
[4] R. Viswanathan, M. Sai Baba, D. Darwin Albert Raj, R. Balasubramanian, B. Saha, C.K. Mathews, J. Nucl. Mater. 167 (1989) 94.
[5] R. Viswanathan, M. Sai Baba, D. Darwin Albert Raj, R. Balasubramanian, B. Saha, C.K. Mathews, J. Nucl. Mater. 149 (1987) 302.
[6] R. Viswanathan, M. Sai Baba, T.S. Lakshmi Narasimhan, R. Balasubramanian, D. Darwin Albert Raj, C.K. Mathews, J. Alloys Compd. 206 (1994) 201.
[7] R. Viswanathan, R. Balasubramanian, C.K. Mathews, J. Chem. Thermodyn. 21 (1989) 1183.
[8] R. Viswanathan, D. Darwin Albert Raj, T.S. Lakshmi Narasimhan, R. Balasubramanian, C.K. Mathews, J. Chem. Thermodyn. 25 (1993) 533.
[9] M. Sai Baba, T.S. Lakshmi Narasimhan, R. Balasubramanian, C.K. Mathews, J. Nucl. Mater. 201 (1993) 147.
[10] T.S. Lakshmi Narasimhan, R. Viswanathan, R. Balasubramanian, J. Phys. Chem. B 102 (1998) 10586.
[11] T.S. Lakshmi Narasimhan, M. Sai Baba, R. Balasubramanian, S. Nalini, R. Viswanathan, J. Chem. Thermodyn. 34 (2002) 103.
[12] B. Saha, R. Viswanathan, M. Sai Baba, C.K. Mathews, High Temperatures-High Pressures 20 (1988) 47.
[13] M. Sai Baba, R. Viswanathan, C.K. Mathews, Rapid Commun. Mass Spectrom. 10 (1996) 691.
[14] T.S. Lakshmi Narasimhan, M. Sai Baba, R. Viswanathan, J. Phys. Chem. B 106 (2002) 6762.
[15] T.S. Lakshmi Narasimhan, M. Sai Baba, S. Nalini, R. Viswanathan, in: C.G.S. Pillai, K.L. Ramkumar, P.V. Ravindran, V. Venugopal (Eds.), Proceedings of the Thirteenth National Symposium on Thermal Analysis, BARC, Mumbai, 2002, pp. 221–222.
[16] M. Von Trömel, D. Schmid, Z. Anorg. Allg. Chem. 387 (1970) 230.
[17] M. Von Trömel, T. Scheller, Z. Anorg. Allg. Chem. 427 (1976) 229.
[18] G. Bayer, Z. Kristallogr. 124 (1967) 131.
[19] Y.Y. Ivanova, Mater. Chem. 7 (1982) 449.
[20] G.G. Gospodinov, D.I. Mihov, J. Chem. Thermodyn. 25 (1993) 1249.
[21] T.S. Lakshmi Narasimhan, R. Balasubramanian, S. Nalini, M. Sai Baba, J. Nucl. Mater. 247 (1997) 28.
[22] PDF-2 Data Base, JCPDS-ICDD, Pensylvania, USA, Copy Right 1987–1994.
[23] T.E. Moore, M. Ellis, P.W. Selwood, J. Am. Chem. Soc. 72 (1950) 856.